East European Journal of Physics. 3. 564-574 (2026)
DOI:10.26565/2312-4334-2026-3-51 ISSN 2312-4334

TEMPERATURE-DRIVEN PHASE EVOLUTION AND LATTICE STRAIN DYNAMICS DURING Ga–Sb CO-DIFFUSION IN SINGLE-CRYSTAL SILICON

Bobir O. Isakov*, Khalmurat M. Iliev, Kutub S. Ayupov, Bakhram A. Abdurakhmanov, Giyosiddin A. Kushiev, Abdujalol A. Sattorov, Zafar B. Khudoynazarov
Tashkent State Technical University, University St., 2, 100095, Tashkent, Uzbekistan
Corresponding Author e-mail: bobir6422isakov@gmail.com
Received June 6, 2026; revised July 27, 2026; in final form August 13, 2026; accepted August 26, 2026

This study examines the effect of annealing temperature on the microstructure and lattice dynamics of single-crystal silicon co-diffused with gallium and antimony. Samples were annealed in the 1000–1250°C range for a fixed duration of 10 h and analyzed by SEM imaging, EDS elemental mapping, and Raman spectroscopy. With increasing temperature, the samples show four successive microstructural states: (I) sparse Ga-rich clustering at 1000°C, (II) formation of large GaSb droplets (25–60 μm) at 1100°C, (III) refinement into smaller, faceted precipitates (~5 μm) at 1200°C, and (IV) substantial re-dissolution of the secondary phase, leaving only residual domains of ~1.5 μm, at 1250°C. Raman measurements of the Si optical phonon track this sequence: a small tensile shift (~518–519 cm^{-1}) at 1000 °C, a return to the unstrained position (~520 cm^{-1}) at 1100°C when GaSb droplets accommodate most of the lattice mismatch, and increasing compressive shifts (524–525 cm^{-1}, corresponding to ~0.6% strain) at 1200–1250°C as the GaSb phase redissolves into the matrix. Phonon-confinement analysis of the Raman linewidth further indicates crystalline coherence lengths of 3–5 nm within the micrometer-scale precipitates. Taken together, these results indicate that annealing temperature governs a reproducible sequence of clustering, droplet segregation, precipitate refinement, and re-homogenization in the Ga–Sb–Si system, and that this sequence can be tracked quantitatively through the correlated SEM/EDS and Raman signatures reported here.
Keywords: *Diffusion; Segregation; Nanocrystalline; Precipitation; Lattice strain; Phase separation*

1. INTRODUCTION

Thermally activated diffusion in silicon constitutes a foundational mechanism in semiconductor device fabrication, enabling dopant activation, junction formation, and heterostructure integration [1-3]. While single-species diffusion is well described by Fickian transport and point-defect mediation [4], multicomponent diffusion introduces additional complexity due to competing thermodynamic and kinetic driving forces, defect interactions, and solute–solute coupling effects [5, 6]. In systems where diffusing species possess mutual chemical affinity and limited solid solubility, diffusion may trigger phase segregation, nanoscale precipitation, interfacial strain generation, and re-equilibration processes governed by temperature-dependent free-energy landscapes [7-9].

The Ga–Sb–Si ternary system represents a prototypical compound-forming diffusion platform. Gallium (Group III) and antimony (Group V) are individually established dopants in silicon technology [10]; however, their simultaneous introduction at elevated temperature can promote GaSb compound formation due to chemical affinity and lattice incompatibility with the Si host matrix [11, 12]. GaSb itself is a narrow-bandgap III–V semiconductor with infrared optoelectronic relevance, making its controlled integration within silicon technologically attractive for monolithic optoelectronic platforms [13, 14].

From a thermodynamic perspective, phase stability is governed by minimization of total Gibbs free energy:

$$\Delta G=\Delta Gv+\gamma A \tag{1}$$

where ΔG is the total change in Gibbs free energy accompanying precipitate formation, ΔG_v is the volumetric (bulk) free-energy term that drives precipitation, γ is the interfacial energy per unit area, and A is the surface area of the forming precipitate.

Precipitation is thermodynamically favorable only when the volumetric term ΔG_v outweighs the interfacial-energy penalty γA [15]. Because temperature modulates diffusion coefficients, solid solubility limits, and the balance between these two terms, it can drive transitions between metastable supersaturation, compound segregation, precipitation refinement, and re-homogenization [16]. In compound-forming systems, nucleation kinetics and strain-driven morphological evolution further influence nanostructure stability [15].

Raman spectroscopy provides a powerful nondestructive probe of strain, phonon confinement, and compositional evolution in semiconductor systems [17–19]. Phonon confinement effects in nanocrystals lead to asymmetric peak broadening and redshift, enabling extraction of crystallite size and strain distribution [18, 19].

A temperature-dependent structural–vibrational correlation for the Ga–Sb–Si system has not yet been established in the literature. The purpose of this work is to study the effect of annealing temperature on the structure of silicon

Cite as: B.O. Isakov, Kh.M. Iliev, K.S. Ayupov, B.A. Abdurakhmanov, G.A. Kushiev, A.A. Sattorov, Z.B. Khudoynazarov, East Eur. J. Phys. 3, 564 (2026), https://doi.org/10.26565/2312-4334-2026-3-51

diffusion-doped with both gallium and antimony. To this end, we investigate Ga–Sb co-diffusion in silicon across 1000–1250°C and identify the resulting transformation sequence:

- Supersaturation-induced clustering (1000°C),
- Droplet-mediated GaSb segregation (1100°C),
- Diffusion-controlled nanocrystalline precipitation (1200°C),
- Re-homogenization and matrix recovery (1250°C).

By correlating SEM/EDS microstructural evolution with Raman-based strain quantification and phonon confinement modeling, we establish a predictive thermodynamic–kinetic model describing phase stability transitions in this compound-forming diffusion system.

2. MATERIALS AND METHODS

To elucidate the thermodynamic–kinetic transformation pathway proposed in the Introduction, a systematic temperature-resolved experimental framework was designed. The methodology was structured to isolate temperature as the primary control parameter governing Ga–Sb phase evolution in silicon, while maintaining constant diffusion duration and comparable boundary conditions. This approach enables direct correlation between diffusion kinetics, phase stability, and vibrational signatures.

2.1. Substrate Selection and Surface Preparation

Single-crystalline Si wafers with (100) orientation were selected due to their technological relevance and well-characterized diffusion behavior. The (100) surface provides predictable point-defect dynamics and stable crystallographic reference for strain analysis, particularly in Raman measurements [20, 21].

To ensure that phase evolution originated solely from thermally activated Ga–Sb diffusion rather than surface contamination or oxide-mediated reactions, the wafers were subjected to a standard RCA cleaning protocol [22]. The process consisted of:

- SC-1 treatment (NH_4OH–H_2O_2–H_2O) for organic removal,
- Dilute HF dip (1–2%) to remove native SiO_2,
- SC-2 treatment (HCl–H_2O_2–H_2O) for metallic impurity elimination.

Such preparation is essential because residual oxides or metallic contaminants can alter interfacial energy and modify diffusion pathways, thereby affecting phase nucleation behavior [23].

2.2. Temperature-Controlled Co-Diffusion of Ga and Sb

Simultaneous diffusion of Ga and Sb was performed in a high-temperature quartz tube furnace under controlled ambient conditions. The diffusion duration was fixed at 10 hours to ensure sufficient atomic redistribution while allowing temperature-dependent phase transitions to manifest distinctly.

Four annealing temperatures were selected:

- 1000°C (Group I),
- 1100°C (Group II),
- 1200°C (Group III),
- 1250°C (Group IV).

The chosen temperature window spans regimes where diffusion kinetics, solid solubility, and compound stability are expected to vary significantly according to Arrhenius behavior:

$$D = D_0 \exp\left(-E_a / kT\right). \tag{2}$$

Here D is the diffusion coefficient, D_0 is the pre-exponential (attempt-frequency) factor, E_a is the activation energy for Ga–Sb diffusion in silicon, k_β is the Boltzmann constant, and T is the absolute annealing temperature. This design allows the system to traverse multiple thermodynamic states—from supersaturation to segregation and re-equilibration—while holding diffusion time constant.

At lower temperature (1000°C), limited atomic mobility favors metastable supersaturation and localized clustering. Increasing temperature enhances vacancy-mediated Ga diffusion and substitutional Sb incorporation [24-27], potentially enabling compound formation and droplet segregation. At the highest temperature (1250°C), increased solid solubility may promote partial re-dissolution of secondary phases, restoring matrix homogeneity [28].

Temperature was monitored with calibrated thermocouples (±2°C accuracy) to minimize thermal gradient effects.

2.3. Microstructural Characterization (SEM)

To track morphological evolution across transformation regimes, field-emission scanning electron microscopy (FE-SEM–JEOL JSM-IT200) was employed. Accelerating voltages between 5 and 15 kV were used to balance surface sensitivity and compositional contrast.

Backscattered electron (BSE) imaging was particularly important for identifying Ga–Sb-rich precipitates due to atomic number contrast enhancement [29]. This technique allows direct visualization of droplet-mediated segregation predicted by the thermodynamic model introduced earlier.

The SEM analysis focused on:

- Precipitate morphology,
- Droplet diameter distribution,
- Surface roughness variation,
- Transition from localized clusters to homogenized matrix.

Spatial resolution was approximately 5 nm under optimized conditions.

2.4. Elemental Mapping (EDS)

Energy-dispersive X-ray spectroscopy (EDS) was integrated with SEM to determine spatial distribution of Ga and Sb.

Elemental mapping enabled:

- Verification of Ga–Sb co-segregation,
- Identification of Ga-rich versus Sb-rich domains,
- Assessment of elemental homogenization at elevated temperature.

Quantitative compositional analysis was performed using ZAF correction procedures to compensate for atomic number, absorption, and fluorescence effects [30]. The correlation between morphological features and elemental concentration provided direct validation of phase segregation or re-dissolution mechanisms.

2.5. Raman Spectroscopy and Vibrational Analysis

To probe lattice dynamics and phase-specific vibrational modes, micro-Raman spectroscopy was performed at room temperature using a 532 nm excitation laser. The spectral range (100–1200 cm^{-1}) captured:

- GaSb TO phonon (~223 cm^{-1}),
- Si optical phonon (~520 cm^{-1}),
- Si–O–Si vibrational modes (~900–1050 cm^{-1}).

Laser power was kept below 5 mW to avoid local heating and peak shift artifacts.

Raman spectroscopy serves a dual purpose in this study:

1. Phase identification (GaSb formation),
2. Quantitative structural assessment via strain and phonon confinement analysis.

2.6. Strain Determination from Raman Peak Shift

The temperature-dependent shift of the Si optical phonon was used to estimate lattice strain according to [31]:

$$\Delta\omega = -830\varepsilon$$

where $\Delta\omega$ is the shift of the Si optical-phonon peak position relative to the strain-free bulk Si reference (520 cm^{-1}) and ε is the resulting biaxial lattice strain (dimensionless, positive values denote tensile strain and negative values compressive strain). This relation enables quantification of compressive or tensile strain induced by GaSb phase formation and interfacial stress.

2.7. Phonon Confinement and Crystallite Size Estimation

To distinguish between micrometer-scale precipitate morphology and nanometer-scale crystalline coherence, the Campbell–Fauchet phonon confinement model was applied [32]:

$$\Gamma(L) = \Gamma_0 + \frac{A}{L^2} \tag{3}$$

where Γ is the Raman linewidth (FWHM), Γ_0 is the intrinsic bulk linewidth, and L is the phonon coherence length.

This approach enables estimation of internal crystallite size independent of precipitate diameter observed by SEM, thus resolving scale-dependent structural effects.

3. RESULTS AND DISCUSSION

The experimental framework described in Section 2 was designed to systematically probe temperature-driven phase evolution in the Ga–Sb–Si ternary system. The results reveal a clear transformation pathway governed by thermodynamic stability and diffusion kinetics. Structural, compositional, and vibrational analyses collectively confirm the four-stage evolution proposed in Section 1.

3.1. Microstructural Evolution Observed by SEM

At 1000°C (Group I), the SEM micrograph (Figure 1a) shows a relatively smooth silicon matrix with localized bright contrast regions. The absence of macroscopic droplet formation indicates that the system remains supersaturated. Such morphology is consistent with early-stage nucleation, in which the volumetric free energy reduction (ΔG_v) is insufficient to overcome interfacial energy penalties (γA) for the formation of large precipitates [33, 34].

The localized bright regions correspond to Ga-rich clusters, suggesting that diffusion has initiated but remains kinetically limited.

At 1100°C, a pronounced morphological transition occurs. SEM (Figure 2a) reveals micrometer-scale spherical precipitates distributed across the surface. The spherical geometry strongly suggests minimization of interfacial energy, characteristic of droplet-mediated phase segregation. This behavior resembles classical liquid-phase separation mechanisms described in alloy systems. The temperature increase enhances atomic mobility according to Arrhenius kinetics, enabling Ga and Sb atoms to coalesce into GaSb-rich domains. The droplet morphology confirms the system has crossed a thermodynamic segregation threshold. The formation of spherical Ga–Sb-rich precipitates and their partial embedding into the Si matrix, shown in the magnified views (Figures 2f–g) and in cross-section (Figures 2h–i), indicates thermally driven droplet-mediated phase separation.

At 1200°C, the large droplet morphology disappears. Instead, finely dispersed precipitates with faceted features emerge (Figure 3a). The faceting indicates crystallographically controlled growth, suggesting a diffusion-limited precipitation regime rather than liquid coalescence. This transition reflects a shift from interfacial-energy-dominated droplet formation to bulk diffusion-controlled phase stabilization.

The reduced particle size and faceted morphology, illustrated by the extended surface views (Figures 3f–g) and by the faceted square-shaped precipitate (Figure 3h), suggest diffusion-controlled nucleation and crystallographically oriented Ga–Sb phase formation.

At 1250°C, precipitates are significantly reduced and the surface regains homogeneity (Figure 4a). This indicates partial re-dissolution of GaSb phases due to increased solid solubility at elevated temperature.

Such behavior is consistent with thermodynamic re-equilibration and reduction of interfacial area.

The absence of large precipitates and the uniform elemental distribution suggest re-dissolution and homogenization of Ga–Sb phases within the Si matrix during advanced thermal processing.

3.2. Elemental Redistribution (EDS Analysis)

EDS elemental mapping further corroborates the morphological interpretations derived from the SEM analysis.

As shown in Figures 1b–f, at 1000°C gallium exhibits pronounced localized clustering, whereas antimony displays a comparatively more diffuse spatial distribution across the silicon matrix. The incomplete spatial overlap between Ga and Sb elemental maps indicates that full GaSb compound formation has not yet occurred at this stage. Instead, the observed partial compositional segregation suggests a metastable supersaturation regime, in which atomic redistribution is initiated but remains insufficient to achieve complete compound stabilization.

This behavior is consistent with diffusion-limited kinetics at 1000°C, where the thermodynamic driving force for phase formation is present, yet interfacial energy barriers and limited atomic mobility prevent extensive co-segregation and long-range ordering.

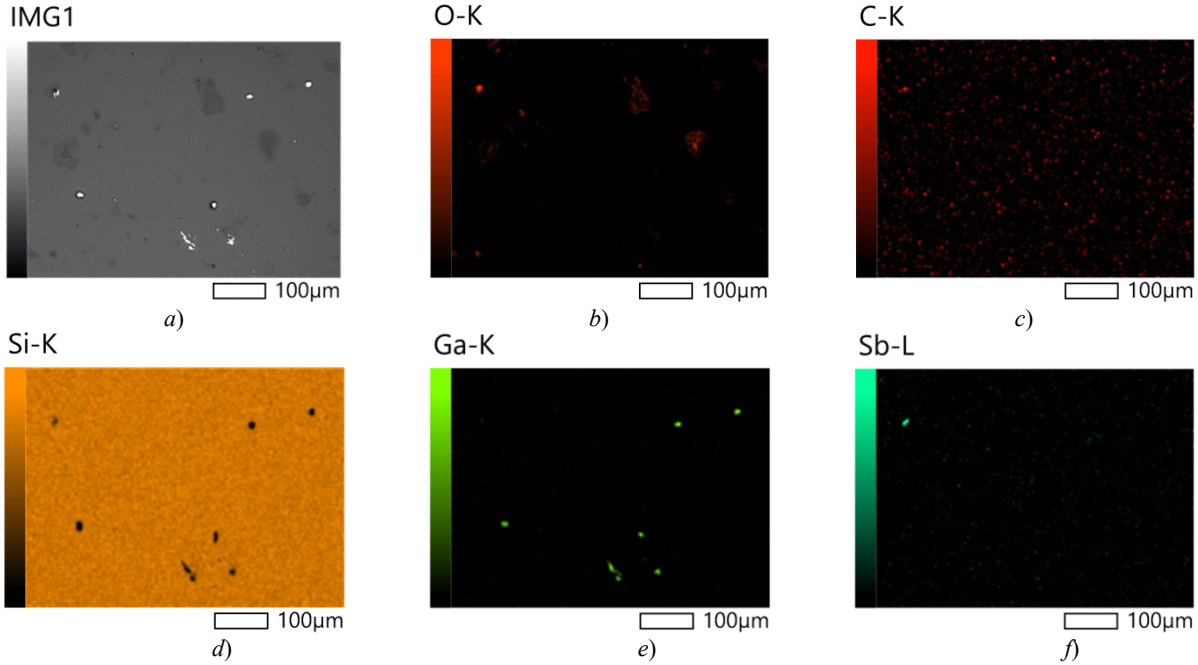

Figure 1. SEM micrographs and EDS elemental mappings of the Group I sample: (a) surface morphology; (b) O–K map; (c) C-K map; (d) Si–K map; (e) Ga–K map; (f) Sb–L map

As shown in Figures 2b–e, at 1100°C gallium and antimony exhibit a pronounced spatial correlation within well-defined spherical droplets distributed across the surface. SEM analysis reveals that the droplets have diameters ranging from approximately 25 to 60 μm, with an average size of about 40 ± 15 μm based on scale-bar estimation.

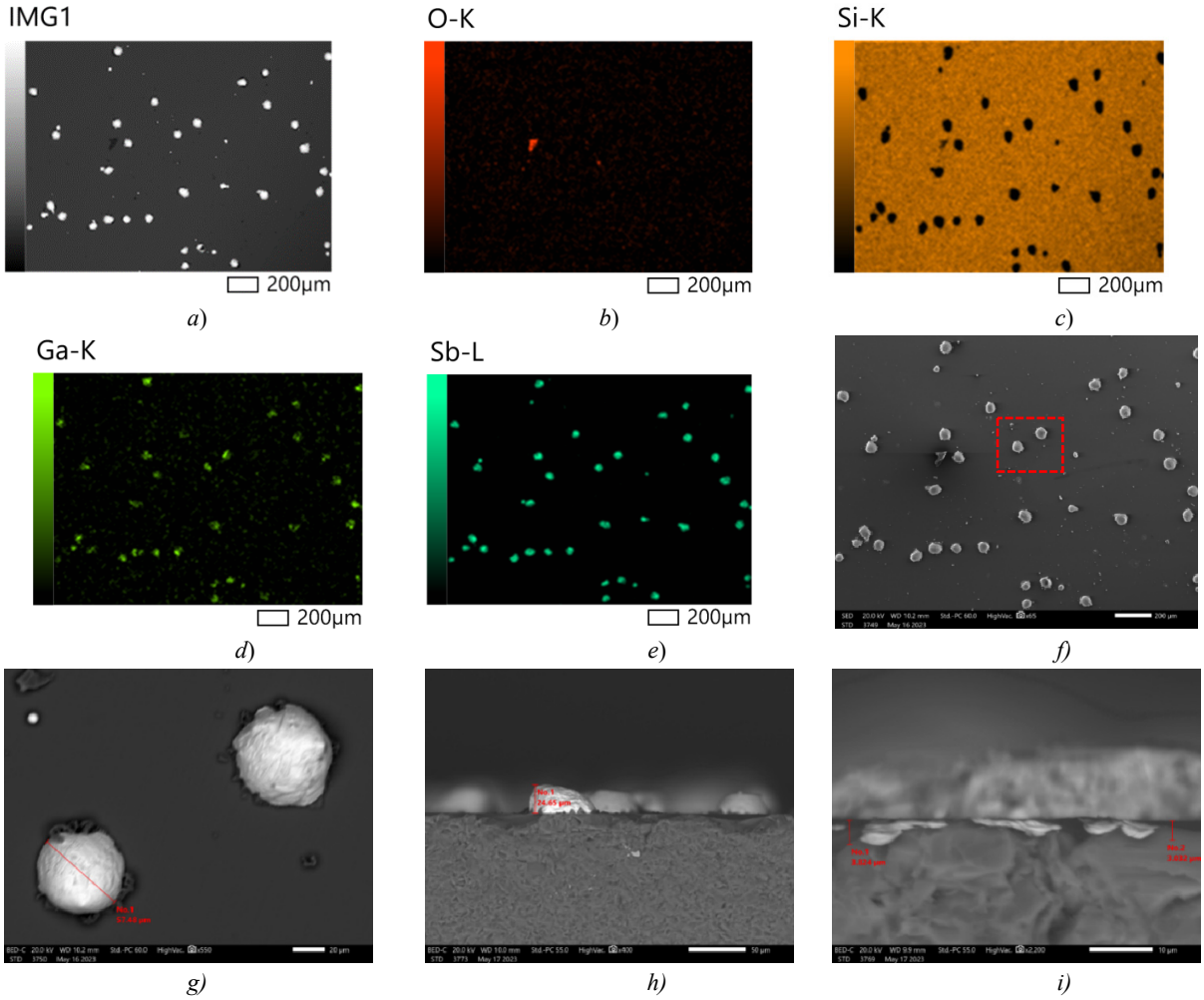

Figure 2. SEM micrographs and EDS elemental mappings of Group II sample: (a) surface morphology; (b) O–K; (c) Si–K; (d) Ga–K; (e) Sb–L; (f–g) magnified precipitate morphology; (h–i) cross-sectional analysis

The nearly complete overlap of Ga and Sb elemental distributions within these micrometer-scale droplets provides direct compositional evidence for GaSb-rich phase formation. The spherical morphology indicates interfacial energy minimization, characteristic of droplet-mediated segregation processes governed by surface tension effects.

The relatively broad size distribution suggests rapid nucleation followed by coarsening dynamics, consistent with classical Ostwald ripening behavior. At this temperature, enhanced atomic mobility enables efficient interdiffusion between Ga and Sb, allowing local compositional equilibrium to be established within individual droplets. The observed behavior aligns with Ga–Sb binary phase diagram predictions, where elevated temperature promotes compound nucleation and thermodynamically stabilized phase segregation.

As observed in Figures 3b–e, at 1200°C gallium and antimony remain spatially correlated; however, their distribution becomes markedly more homogeneous compared to the pronounced droplet segregation observed at 1100°C. The elemental maps reveal that Ga–Sb-rich regions are no longer confined to large spherical droplets but instead appear as finely dispersed, micrometer-scale precipitates distributed throughout the silicon matrix.

SEM analysis (50 μm scale) indicates that the bright islands exhibit characteristic lateral dimensions ranging from approximately 2 to 10 μm, with an average diameter of about 5 ± 3 μm. This represents a significant refinement compared to the 25–60 μm droplets observed at 1100°C. The reduction in island size, combined with an increased areal density, suggests fragmentation and redistribution rather than continued coalescence.

The Ga–K and Sb–L maps demonstrate strong local compositional overlap within these smaller precipitates, confirming the persistence of GaSb-rich phase domains. However, the improved spatial uniformity and absence of large spherical droplets indicate that interfacial-energy-driven segregation is no longer the dominant mechanism. Instead, bulk diffusion and crystallographically controlled precipitation govern the phase stabilization process.

The partial faceting of several islands further supports a diffusion-limited growth regime, where anisotropic surface energy and lattice accommodation effects influence morphology. The microstructural refinement at 1200°C therefore reflects a transition from droplet-mediated coalescence to diffusion-controlled nanocrystalline precipitation.

Thermodynamically, this stage corresponds to enhanced atomic mobility enabling redistribution of segregated species, while kinetically, the system approaches a more stable, spatially dispersed phase configuration. The observed

decrease in precipitate size and improved compositional homogeneity is consistent with diffusion-driven reorganization and internal domain stabilization.

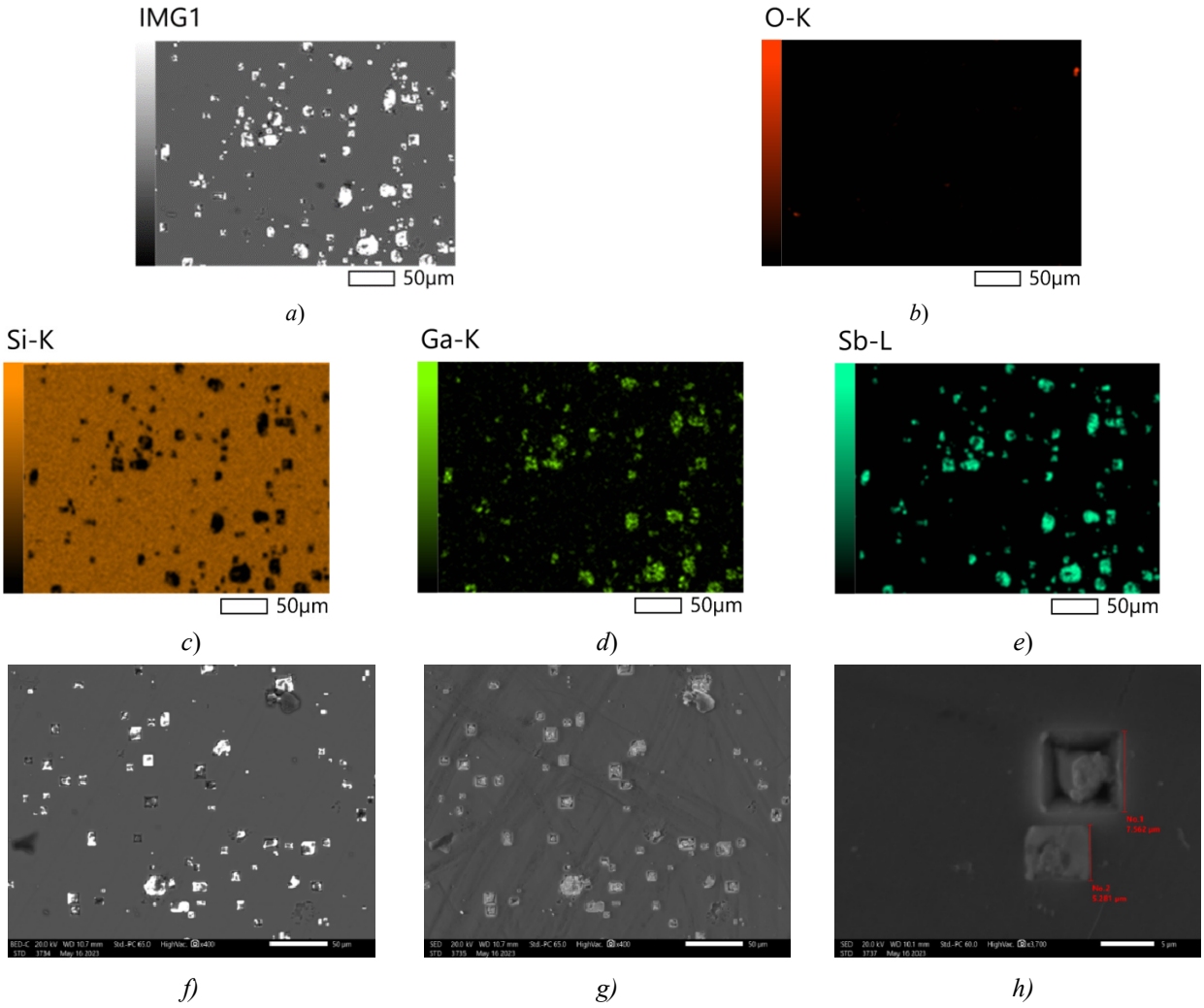

Figure 3. SEM micrographs and EDS elemental mappings of Group III sample:(a) surface morphology; (b) O–K; (c) Si–K; (d) Ga–K; (e) Sb–L; (f–g) extended surface morphology; (h) faceted square-shaped precipitate

Overall, the structure at 1200°C represents an intermediate equilibrium regime characterized by:

- Reduced precipitate size (≈5 μm average),
- Increased spatial dispersion,
- Strong Ga–Sb compositional correlation,
- Suppression of large droplet morphology,
- Diffusion-limited precipitation dynamics.

This regime provides clear experimental evidence of the thermodynamic–kinetic shift from segregation-dominated growth (1100°C) to controlled nanocrystalline stabilization.

As shown in Figures 4b–f, at 1250°C the elemental distributions of Ga and Sb become significantly more homogeneous across the silicon matrix compared to the lower-temperature samples. The Ga–K and Sb–L maps show only weak, sparsely distributed localized intensity maxima, indicating a substantial reduction in segregated GaSb-rich domains.

SEM analysis (10 μm scale) reveals that the previously observed micrometer-scale precipitates have largely disappeared. The remaining bright features appear as small residual islands with characteristic lateral dimensions ranging from approximately 0.5 to 3 μm, with an average effective diameter of about 1.5 ± 0.8 μm. The areal density of these islands is markedly reduced relative to both the 1100°C and 1200°C conditions.

The significant decrease in island size and density, together with the reduced compositional contrast in the Ga and Sb maps, strongly indicates partial re-dissolution of the GaSb-rich phase into the silicon matrix. The near-uniform Si–K signal further confirms matrix recovery and suppression of compositional segregation.

Thermodynamically, this behavior reflects increased solid solubility and entropy-driven redistribution at elevated temperature. Kinetically, the enhanced diffusion coefficients at 1250°C promote homogenization rather than further

precipitate growth. The absence of large droplets and the emergence of only sub-micrometer residual domains demonstrate that interfacial energy is no longer the dominant driving force; instead, bulk diffusion and equilibrium solubility limit phase persistence.

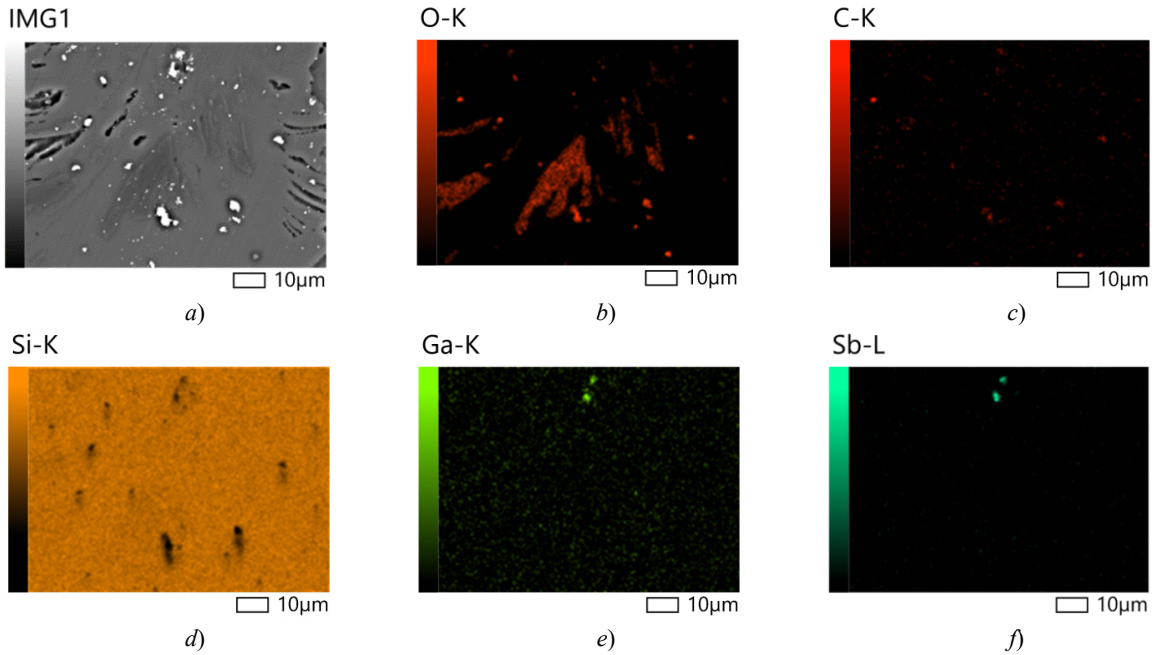

Figure 4. SEM micrographs and EDS elemental mappings of Group IV sample: (a) surface morphology; (b) O–K; (c) C–K; (d) Si–K; (e) Ga–K; (f) Sb–L

Overall, the microstructure at 1250°C represents a re-homogenization regime characterized by:

- Strongly reduced precipitate size (~1.5 μm average),
- Low areal density of residual islands,
- Weak Ga–Sb compositional localization,
- Restoration of silicon matrix continuity.

This stage marks the final thermodynamic stabilization of the system, completing the transformation pathway from supersaturation (1000°C) through segregation (1100°C) and diffusion-limited precipitation (1200°C) to matrix recovery at 1250°C.

3.3. Raman Spectral Evolution

As observed in Figure 5, the Raman spectrum of the Group I sample exhibits a slight downshift of the Si optical phonon to approximately 518–519 cm^{-1}, corresponding to an estimated tensile strain of ~0.18%. This negative peak shift relative to the stress-free crystalline silicon position (520 cm^{-1}) indicates minor lattice expansion, most likely due to the substitutional incorporation of diffusing species within the Si matrix.

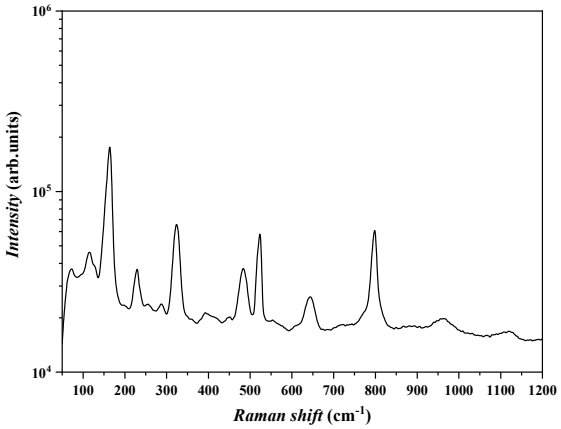

Figure 5. Raman spectrum of the Group I sample (1000°C, 10 h annealing)

The absence of a dominant GaSb transverse optical (TO) mode near 223 cm^{-1}, together with the presence of broad disorder-induced bands in the low-wavenumber region, suggests incomplete compound formation and limited Ga–Sb co-segregation. Instead of forming well-defined GaSb-rich droplets, the diffusing species appear to remain partially incorporated within the silicon lattice.

This vibrational behavior is consistent with the SEM/EDS observations of Group I (1000°C), where sparsely distributed micrometer-scale Ga-rich islands (~7 μm) were detected with incomplete Sb overlap. The low areal density of these islands and the lack of strong compositional correlation confirm that the system remains in a metastable supersaturation regime. Under these conditions, lattice distortion originates primarily from localized substitutional incorporation and early-stage clustering rather than from macroscopic droplet segregation.

The combined structural and vibrational evidence therefore conclusively identifies this spectrum as corresponding to the supersaturation regime at 1000°C.

As observed in Figure 6, the Raman spectrum exhibits a pronounced and well-defined GaSb transverse optical (TO) phonon mode at approximately 223 cm^{-1}, accompanied by a sharp and intense Si–Si optical phonon peak centered near 520 cm^{-1}. The strong GaSb signal indicates substantial compound formation and confirms effective co-segregation of Ga and Sb at this annealing temperature.

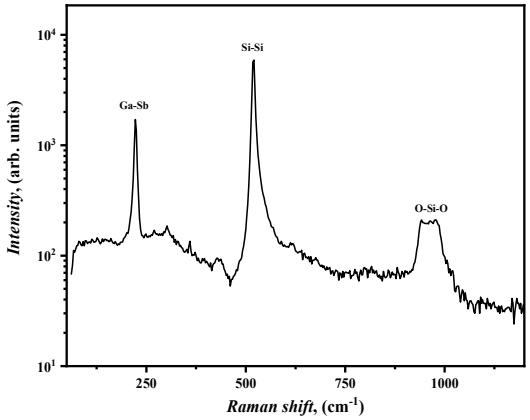

Figure 6. Raman spectrum of the Group II sample (1100°C, 10 h annealing)

Notably, the Si optical phonon peak remains essentially unshifted relative to the stress-free crystalline silicon reference (520 cm^{-1}), suggesting negligible residual lattice strain within the silicon matrix. This absence of measurable peak displacement implies that the segregated GaSb phase has formed discrete micrometer-scale droplets, thereby relieving internal stress that would otherwise accumulate through substitutional incorporation.

The moderate disorder background and the presence of a secondary O–Si–O band in the 900–1000 cm^{-1} region are consistent with interface-related vibrational contributions and minor surface oxidation, rather than bulk structural distortion. This vibrational behavior is consistent with the SEM/EDS observations of Group II (1100°C), where large spherical droplets (approximately 25–60 μm in diameter) with strong Ga–Sb compositional overlap were detected. The formation of these well-defined GaSb-rich domains represents a thermodynamically stabilized segregation regime, in which interfacial energy minimization dominates over lattice incorporation mechanisms.

Therefore, the combined structural and vibrational evidence indicates that this Raman spectrum corresponds to the droplet-mediated segregation stage at 1100°C.

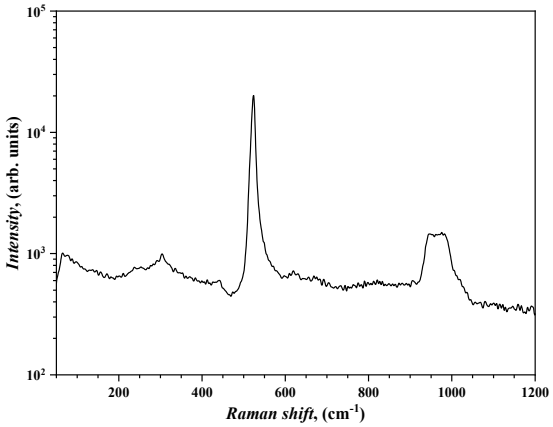

Figure 7. Raman spectrum of the Group III sample (1200°C, 10 h annealing).

As observed in Figure 7, the Raman spectrum is dominated by a pronounced Si–Si optical phonon peak located at approximately 524 cm^{-1}, indicating a measurable upshift relative to the stress-free crystalline silicon reference at 520 cm^{-1}. This positive shift corresponds to an estimated compressive strain of ~0.48–0.50%, calculated using the phonon deformation potential relationship ($\Delta\omega = -830\varepsilon$). The observed peak displacement signifies enhanced lattice distortion compared to both the 1000°C and 1100°C conditions.

In contrast to the strong and sharp GaSb TO mode observed at 1100°C, the low-wavenumber region in this spectrum exhibits only weak and broadened features, suggesting a reduced effective GaSb phase fraction. The absence of a dominant, narrow GaSb peak indicates that large droplet segregation is no longer the prevailing mechanism.

The moderate broadening of the Si phonon peak and the presence of a weak disorder-related background further support the presence of internal stress fields and nanoscale structural heterogeneity. Additionally, the broad band in the 920–1000 cm^{-1} region (Si–O–Si and second-order scattering contributions) reflects interface-related vibrational activity rather than bulk oxidation. This vibrational behavior is consistent with the SEM/EDS observations of Group III (1200°C), where the previously large micrometer-scale droplets disappear and are replaced by refined precipitates with characteristic sizes of approximately 2–10 μm (average ~5 μm). The increased spatial dispersion and reduced precipitate size indicate a transition from interfacial-energy-dominated segregation to diffusion-limited nanocrystalline precipitation.

The significant compressive strain observed at 1200°C arises from partial redistribution of Ga and Sb within the silicon matrix and enhanced lattice accommodation during phase refinement. Therefore, the combined structural and vibrational evidence indicates that this Raman spectrum corresponds to the diffusion-controlled precipitation regime at 1200°C.

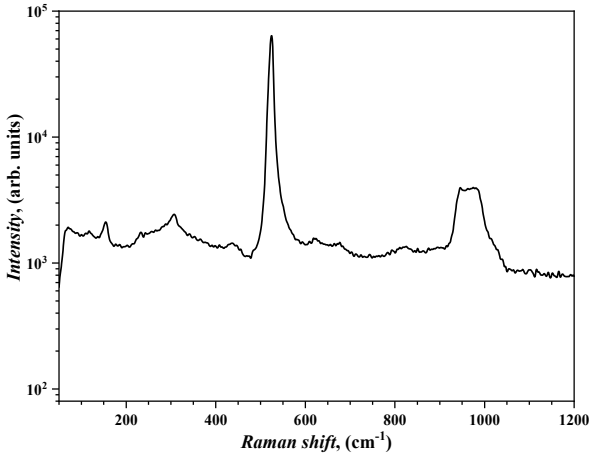

Figure 8. Raman spectrum of the Group IV sample (1250°C, 10 h annealing)

As observed in Figure 8, the Raman spectrum is dominated by a strongly upshifted Si–Si optical phonon peak positioned near 525 cm^{-1}, representing the highest frequency among all investigated samples. Relative to the stress-free silicon reference at 520 cm^{-1}, this corresponds to an estimated compressive strain of approximately ~0.6%, calculated using the phonon deformation potential relationship ($\Delta\omega = -830\varepsilon$). This pronounced peak shift indicates substantial lattice distortion within the silicon matrix. In contrast to the spectrum obtained at 1100°C, the GaSb transverse optical (TO) mode near 223 cm^{-1} is significantly weakened or nearly suppressed, indicating a marked reduction in segregated GaSb-rich phase fraction. The low-wavenumber region shows only minor residual features, suggesting that large-scale compound domains are no longer present.

The moderate broad band in the 920–1000 cm^{-1} range, associated with Si–O–Si vibrations and second-order scattering processes, reflects interface-related vibrational contributions rather than dominant bulk phase formation. The overall spectral profile is cleaner than that observed at 1200°C, indicating reduced nanoscale heterogeneity and enhanced matrix continuity.

This vibrational behavior is consistent with the SEM/EDS observations of Group IV (1250°C), where micrometer-scale precipitates were largely eliminated and only small residual islands (~0.5–3 μm, average ~1.5 μm) remained with significantly reduced areal density. The homogenized elemental distribution confirms partial re-dissolution of GaSb phases into the silicon matrix.

The increased compressive strain at this temperature arises from redistribution of Ga and Sb species into the Si lattice following droplet dissolution. Without large segregated domains to relieve internal stress, the silicon matrix accommodates compositional distortion, leading to the maximum observed phonon upshift.

Therefore, the combined structural and vibrational evidence indicates that this Raman spectrum corresponds to the re-homogenization regime at 1250°C.

4. CONCLUSIONS

This work shows that annealing temperature governs a reproducible sequence of structural and vibrational changes in the Ga–Sb–Si ternary system. Combining SEM, EDS, and Raman spectroscopy, we identify four temperature-dependent regimes: supersaturation (1000°C), droplet-mediated segregation (1100°C), diffusion-limited precipitation (1200°C), and re-homogenization (1250°C).

The structural transition from sparse Ga-rich islands to large GaSb droplets, followed by precipitate refinement and eventual dissolution, is directly mirrored in the vibrational response of the silicon lattice. The non-monotonic evolution of

the GaSb TO mode and the systematic shift of the Si optical phonon from tensile (~0.18%) to maximum compressive strain (~0.6%) provide quantitative evidence of thermodynamic stabilization and kinetic redistribution processes.

The strongest GaSb formation coincides with strain relief at 1100°C, whereas higher temperatures promote phase dissolution and lattice distortion associated with compositional reintegration. This relationship between segregation-driven stress relaxation and homogenization-induced strain accumulation points to a coupling between phase morphology and phonon dynamics in this compound-forming diffusion system, which merits further investigation, for example through in-situ or time-resolved measurements.

These observations provide a basis for a thermodynamic–kinetic description of temperature-controlled heterophase formation in silicon. The ability to move between metastable clustering, stabilized compound domains, refined nanocrystalline precipitation, and near-equilibrium homogenization by varying annealing temperature suggests a route toward strain tuning and embedded III–V phase integration within Si-compatible architectures, though further work is needed to establish the practical limits of this approach.

These findings extend the description of classical diffusion behavior to a multi-component, compound-forming system and offer design considerations for thermally engineered semiconductor structures. By correlating morphology, composition, and lattice dynamics across multiple length scales, this work contributes to the understanding of compound-forming diffusion in silicon and points to potential pathways for phase-functional materials compatible with existing microelectronic technologies.

ORCID

Bobir O. Isakov, https://orcid.org/0000-0002-6072-3695

REFERENCES

[1] S.M. Sze, and K.K. Ng, *Physics of Semiconductor Devices*, 3rd ed., (Wiley, 2007). https://doi.org/10.1002/0470068329
[2] C. Barri, E. Mafakheri, L. Fagiani, G. Tavani, A. Barzaghi, D. Chrastina, A. Fedorov, *et al*., "Engineering of the spin on dopant process on silicon on insulator substrate," Nanotechnology, **32**, 025303 (2021). https://doi.org/10.1088/1361-6528/abbdda
[3] P.M. Fahey, P. B. Griffin, and J. D. Plummer, "Point defects and dopant diffusion in silicon," Rev. Mod. Phys. **61**, 289–384 (1989). https://doi.org/10.1103/RevModPhys.61.289
[4] Y. Su, D. Saric, G. Guevara-Carrion, Y. Zhang, M. He, and J. Vrabec, "Fick and Maxwell-Stefan diffusion of the liquid mixture cyclohexane+toluene+ acetone+ methanol and its subsystems", Chemical Engineering Science, **301**, 120662 (2025). https://doi.org/10.1016/j.ces.2024.120662
[5] M. Bonvalet-Rolland, T. Philippe, and J. Ågren, "Kinetic theory of nucleation in multicomponent systems: An application of the thermodynamic extremum principle", Acta Materialia, **171**(1), 1-7 (2019). https://doi.org/10.1016/j.actamat.2019.03.031
[6] Kh.M. Iliev, N.F. Zikrillaev, K.S. Ayupov, B.O. Isakov, B.A. Abdurakhmanov, Z.N. Umarkhodjaeva, and L.I. Isamiddinova, "Effect of GaSb Compound on Silicon Bandgap Energy", J. Nano- Electron. Phys. **16**(1), 01007 (2024). https://doi.org/10.21272/jnep.16(2).02004
[7] G.P. Edmundo, K.R. Tanya, and R.N. Jonathan, "Design and Applications of Water-Soluble Coordination Cages," Chem. Rev. **120**, 13480−13544 (2020). http://dx.doi.org/10.1021/acs.chemrev.0c00672
[8] S. Yi, J.-S. Chen, C.-M. Wang, and W.-S. Liao, "Manipulating Chemical Processes by Pseudosolid Spatial Limitation", JACS Au, **1**(9): 1435–1444 (2021). https://doi.org/10.1021/jacsau.1c00202
[9] E. Guzmán, F. Martínez-Pedrero, C. Calero, A. Maestro, F. Ortega, and R.G. Rubio, "A broad perspective to particle-laden fluid interfaces systems: from chemically homogeneous particles to active colloids", Advances in Colloid and Interface Science, **302**, 102620 (2022). https://doi.org/10.1016/j.cis.2022.102620
[10] N.F. Zikrillayev, S.B. Isamov, B.O. Isakov, T. Wumaier, L.W. Liang, J.X. Zhan, and T. Xiayimulati, "New Technological Solution for the Tailoring of Multilayer Silicon-based Systems with Binary Nanoclusters Involving Elements of Groups III and V," J. Nano- Electron. Phys. **15**, 06024 (2023). https://doi.org/10.21272/jnep.15(6).06024
[11] X.M. Iliyev, S.B. Isamov, B.O. Isakov, U.X. Qurbonova, and S.A. Abduraxmonov, "A surface study of Si doped simultaneously with Ga and Sb," East European Journal of Physics, (3), 303-307 (2023). https://doi.org/10.26565/2312-4334-2023-3-29
[12] X.M. Iliyev, V.B. Odzhaev, S.B. Isamov, B.O. Isakov, B.K. Ismaylov, K.S. Ayupov, and Sh.I. Hamrokulov, "X-ray diffraction and Raman spectroscopy analyses of GaSb-enriched Si surface formed by applying diffusion doping technique," East Eur. J. Phys. (3), 363-369 (2023), https://doi.org/10.26565/2312-4334-2023-3-38
[13] Kh.M. Iliev, S.V. Koveshnikov, B.O. Isakov, E.Zh. Kosbergenov, G.A. Kushiev, and Z.B. Khudoynazarov, "The Elemental Composition Investigation of Silicon Doped with Gallium and Antimony Atoms," Surface Engineering and Applied Electrochemistry, **60**(4), 633–639 (2024). https://doi.org/10.3103/S106837552470025X
[14] S.K. Madisetti, V. Tokranov, A. Greene, S. Novak, M. Yakimov, S. Oktyabrsky, S. Bentley, and A.P. Jacob, "GaSb on Si: Structural Defects and Their Effect on Surface Morphology and Electrical Properties," Mater. Res. Soc. Symp. Proc. **1635**, (2014). https://doi.org/10.1557/opl.2014.219
[15] J. Gebauer, M. Lausmann, F. Redmann, R. Krause-Rehberg, H.S. Leipner, E.R. Weber, and Ph. Ebert, "Determination of the Gibbs free energy of formation of Ga vacancies in GaAs by positron annihilation," Physical Review B, **67**, 235207 (2003), https://doi.org/10.1103/PhysRevB.67.235207
[16] Shuo Liu, Chaochao Dun, Jeffrey J. Urban, Mark T. Swihart, "Non-Equilibrium Synthesis Methods to Create Metastable and High-Entropy Nanomaterials," Advanced Science, **13**, e21953 (2026). https://doi.org/10.1002/advs.202521953
[17] A. Orlando, F. Franceschini, C. Muscas, S. Pidkova, M. Bartoli, M. Rovere, and A. Tagliaferro, "A Comprehensive Review on Raman Spectroscopy Applications," Chemosensors, **9**, 262 (2021). https://doi.org/10.3390/chemosensors9090262
[18] X. Cong, X.-L. Liu, M.-L. Lin, and P.-H. Tan, "Application of Raman spectroscopy to probe fundamental properties of two-dimensional materials," npj 2D Materials and Applications, **13**, (2020). https://doi.org/10.1038/s41699-020-0140-4

[19] G. La Penna, C. Mancini, A. Proietti, L. Buccini, D. Passeri, N. Gambacorti, J. Richy, and M. Rossi, "Strained Silicon Technology: Non-Destructive High-Lateral-Resolution Characterization Through Tip-Enhanced Raman Spectroscopy," Applied Spectroscopy, **78**(12) 1245–1255 (2024). https://doi.org/10.1177/00037028241246292
[20] W. O'Leary, M. Grumet, W. Kaiser, T. Bucko, J.L. M. Rupp, and D.A. Egger, "Rapid Characterization of Point Defects in Solid-State Ion Conductors Using Raman Spectroscopy, Machine-Learning Force Fields, and Atomic Raman Tensors," J. Am. Chem. Soc. **146**, 26863−26876 (2024). https://doi.org/10.1021/jacs.4c07812
[21] G. Gouadec, and P. Colomban, "Raman Spectroscopy of Nanomaterials: How Spectra Relate to Disorder, Particle Size and Mechanical Properties," Progress in Crystal Growth and Characterization of Materials, **53**(1), 1-56 (2007). https://doi.org/10.1016/j.pcrysgrow.2007.01.001
[22] P.V. Pham, T.-H. Mai, S.P. Dash, V. Biju, Y.-L. Chueh, D. Jariwala, and V. Tung, "Transfer of 2D Films: From Imperfection to Perfection," ACS Nano, **18**, 14841−14876 (2024). https://doi.org/10.1021/acsnano.4c00590
[23] G. Gyarmati, and J. Erdélyi, "Intermetallic Phase Control in Cast Aluminum Alloys by Utilizing Heterogeneous Nucleation on Oxides," Metals, **15**, 404 (2025). https://doi.org/10.3390/met15040404
[24] S. Barth, M.S. Seifner, and S. Maldonado, "Metastable Group IV Allotropes and Solid Solutions: Nanoparticles and Nanowires," Chem. Mater. **32**, 2703−2741 (2020). https://dx.doi.org/10.1021/acs.chemmater.9b04471
[25] A.P. Arun, N. Sreenivasan, J.H. Patil, R. Kusanur, H.L. Ramachandraiah, and M. Ramakrishna, "Thin Films for Next Generation Technologies: A Comprehensive Review of Fundamentals, Growth, Deposition Strategies, Applications, and Emerging Frontiers," Processes, **13**, 3846 (2025). https://doi.org/10.3390/pr13123846
[26] A. Giunto, A. Fontcuberta i Morral, "Defects in Ge and GeSn and their impact on optoelectronic properties," Appl. Phys. Rev. **11**, 041333 (2024). https://doi.org/10.1063/5.0218623
[27] J. Ponis, S. Hariyani, G. Agbeworvi, S. Chakraborty, V. Balcorta, J. Pérez-Vázquez, B.L. Rogers, *et al*., "Single Crystals of Vanadium Oxides as a Lens for Understanding Structural and Electronic Phase Transformations, Ion Transport, Chemo-Mechanical Coupling, and Electrothermal Neuronal Emulation," Chem. Rev. **125**, 10657−10764 (2025). https://doi.org/10.1021/acs.chemrev.5c00413
[28] A. Zaitsev, N. Arutyunyan, and A. Koldaev, "Hot Ductility, Homogeneity of the Composition, Structure, and Properties of High-Strength Microalloyed Steels: A Critical Review," Metals, **13**, 1066 (2023). https://doi.org/10.3390/met13061066
[29] A.A. Ilie, F. Niculescu, G. Iacob, I. Pencea, F. Miculescu, R. Bololoi, D.-V. Drăgut, *et al*., "Microstructure and Properties of Bi-Sn, Bi-Sn-Sb, and Bi-Sn-Ag Solder Alloys for Electronic Applications," Metals, **15**, 915 (2025). https://doi.org/10.3390/met15080915
[30] W.-J. Moon, S.G. Yu, Y.S. Kim, B.-K. Park, W.-G. Jung, and H.-J. Song, "New strategy to improve the accuracy of quantitative analysis of energy dispersive spectroscopy," Phys. Scr. **99**, 035013, (2024). https://doi.org/10.1088/1402-4896/ad241e
[31] M. Xie, M. Li, L. Li, J. Zhang, K. Jiang, L. Shang, Y. Li, *et al*., "Temperature-dependent phonon mode and interband electronic transition evolutions of e-InSe films derived by pulsed laser deposition," Appl. Phys. Lett. **117**, 102101 (2020). https://doi.org/10.1063/5.0021330
[32] S. Marola, S. Bosia, A. Veltro, G. Fiore, D. Manfredi, M. Lombardi, G. Amato, *et al*., "Residual stresses in additively manufactured AlSi10Mg: Raman spectroscopy and X-ray diffraction analysis," Materials and Design **202**, 109550 (2021). https://doi.org/10.1016/j.matdes.2021.109550
[33] M. Perez, M. Dumont, and D. Acevedo-Reyes, "Implementation of the classical nucleation theory for precipitation," Acta Materialia, **56**(9), 2119-2132 (2008). https://doi.org/10.1016/j.actamat.2007.12.050
[34] W. Wełnic, and M. Wuttig, "Reversible switching in phase-change materials," Materials today, **11**(6), (2008). https://doi.org/10.1016/S1369-7021(08)70118-4

ТЕМПЕРАТУРНО-ЗУМОВЛЕНА ФАЗОВА ЕВОЛЮЦІЯ ТА ДИНАМІКА ДЕФОРМВЦІЇ ҐРАТКИ ПІД ЧАС СПІЛЬНОЇ ДИФУЗІЇ Ga–Sb У МОНОКРИСТАЛІЧНОМУ КРЕМНІЇ

Бобір О. Ісаков, Халмурат М. Ілієв, Кутуб С. Аюпов, Бахрам А. Абдурахманов, Гіосіддін А. Кушієв, Абдуджалол А. Сатторов, Зафар Б. Худуйназаров

Ташкентський державний технічний університет, вул. Університетська, 2, 100095, Ташкент, Узбекистан

У цьому дослідженні розглядається вплив температури відпалу на мікроструктуру та динаміку ґратки монокристалічного кремнію, що кодифузувався з галієм та сурмою. Зразки відпалювали в діапазоні 1000–1250°C протягом фіксованої тривалості 10 годин та аналізували за допомогою SEM-візуалізації, EDS-елементного картування та раманівської спектроскопії. Зі зростанням температури зразки демонструють чотири послідовні мікроструктурні стани: (I) розріджене кластеризування, багате на Ga, при 1000°C, (II) утворення великих крапель GaSb (25–60 мкм) при 1100°C, (III) подрібнення на менші, огранованні осади (~5 мкм) при 1200°C та (IV) суттєве повторне розчинення вторинної фази, залишаючи лише залишкові домени розміром ~1,5 мкм, при 1250°C. Раманівські вимірювання оптичних фононів Si відстежують цю послідовність: невеликий зсув на розтяг (~518–519 $см^{-1}$) при 1000°C, повернення до недеформованого положення (~520 $см^{-1}$) при 1100°C, коли краплі GaSb компенсують більшу частину невідповідності кристалічної решітки, та збільшення зсувів на стиск (524–525 $см^{-1}$, що відповідає ~0,6% деформації) при 1200–1250°C, коли фаза GaSb повторно розчиняється в матриці. Аналіз фононного утримання ширини лінії Рамана додатково вказує на довжини кристалічної когерентності 3–5 нм у межах мікрометрових преципітатів. У сукупності ці результати вказують на те, що температура відпалу визначає відтворювану послідовність кластеризації, сегрегації крапель, подрібнення преципітатів та повторної гомогенізації в системі Ga–Sb–Si, і що цю послідовність можна кількісно відстежити за допомогою корельованих SEM/EDS та раманівських сигнатур, про які тут повідомляється.

Ключові слова: *дифузія; сегрегація; нанокристалічний матеріал; осадження; деформація кристалічної решітки; фазове розділення*